Corrosion Science 65 (2012) 556–560

Contents lists available at SciVerse ScienceDirect

Corrosion Science

journal homepage: www.elsevier.com/locate/corsci

The corrosion potential of stainless steel rebars in concrete: Temperature effect

J.M. Deus [a], L. Freire [a,b], M.F. Montemor [b], X.R. Nóvoa [a,*]

[a] ENCOMAT Group, Universidade de Vigo, E.E.I., Campus Universitario, 36310 Vigo, Spain
[b] ICEMS, Instituto Superior Técnico, UTL, Av. Rovisco Pais, 1049-001 Lisbon, Portugal

ARTICLE INFO

Article history:
Received 4 April 2012
Accepted 3 September 2012
Available online 12 September 2012

Keywords:
C. Corrosion potential
A. Steel reinforced concrete
A. Stainless steel
C. Passivity

ABSTRACT

This work reports the temperature dependence of the corrosion potential of passive stainless steel rebars embedded in concrete or in alkaline media. The corrosion potential mirrored the temperature variations and the coefficient (mV/°C) increased as the average temperature range increased. These variations were observed in the long time-scale domain (several hours) and were interpreted based on temperature-induced changes in the chemistry of the passive layer. This behaviour and its interpretation have not been reported before and are of great importance from the point of view of understanding the electrochemical behaviour of stainless steel rebars and the inspection and durability of reinforced concrete structures.

1. Introduction

Passivity of metals involves both coupled chemical and electrochemical phenomena. The growth of the passive film is due to a potential gradient between the metal and the solution, while its dissolution rate depends on both the hydrodynamics at the interface's electrolyte side and the solubility of the oxides/hydroxides composing the passive film. Thus, the stability of the passive film is the result of a compromise between two kinetic processes: film growth and film dissolution [1]. In this context, temperature appears to be a relevant parameter in the stability of passive films. Several approaches have been proposed to account for such effect. Since the pioneering works in the 1970s [2,3], the critical pitting temperature test has been widely employed for evaluating the pitting resistance of stainless steels [4] and is the sole test incorporated into standard practices [5]. The so-called *cyclic thermammetry* technique has also been employed to study the critical repassivation temperature of aluminium in nitric acid solution [6] and temperature transients either under potentiostatic control have also been described as useful thermal technique for passivity studies in Ni-based alloys [7].

The aforementioned methodologies are based on either potentiostatic or galvanostatic control of the metal-solution interface. However, references on the effect of temperature in the corrosion potential are scarce, and only a detailed description is given for a Ni-base alloy [8].

Concerning the behaviour of steel reinforcements in concrete, some literature exists on the effect of temperature on the corrosion rate under isothermal conditions [9,10]. The effect of variable conditions (climatic parameters) has also been studied [11]. However, these works do not report analytical studies and its further correlation to the electrochemical data obtained in quasi-real time at varying temperature. All the published studies to date are limited to phenomenological descriptions of the various environmental effects and no attempts were made to deeper correlate the films composition with its electrochemical response under temperature variations. Thus, the present study focus on the analysis of the free corrosion potential fluctuations induced by temperature changes, providing new insights concerning the role of temperature on the electrochemical response of stainless steel rebars. Field and laboratory experiences combined with an XPS study allow at understanding this phenomenon and its implications in the field of corrosion monitoring of steel reinforced concrete.

2. Experimental

Experiments were conducted in the laboratory and in a field exposure site, a pool of 1.5 m × 1.5 m base dimension and 1.5 m high, located at the seaside under flowing seawater, where the reinforced probes under test were submerged. AISI 304 stainless steel ribbed rods (ϕ = 10 mm) were employed as the testing material. The rebars, having a lateral surface of 30 cm^2 were buried in mortar probes. The mortar samples were prepared using Portland cement (CEM I 52.5 R) with a water-to-cement ratio = 1:2, and a cement-to-sand ratio = 1:3. The probes were cast in cylindrical moulds to produce testing probes of 10 cm diameter and 20 cm height and cured in 100% RH atmosphere at 22 ± 2 °C for at least 1 month before being transferred to the test site.

* Corresponding author. Tel.: +34 986812213; fax: +34 986812201.
E-mail address: rnovoa@uvigo.es (X.R. Nóvoa).

0010-938X/$ - see front matter © 2012 Elsevier Ltd. All rights reserved.
http://dx.doi.org/10.1016/j.corsci.2012.09.001

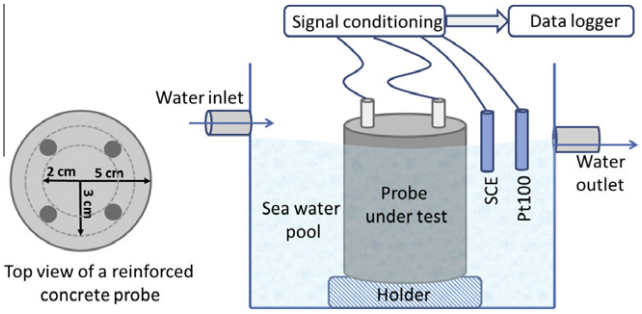

Fig. 1. Schematic representation of the distribution of the reinforcements (solid circles on the left figure) and the distribution of tested probes in the sea water pool. The locations of the reference electrode, SCE, and temperature sensor (Pt100) are also indicated, together with the electrical wiring.

The geometry of the probes and the positioning of the electrodes in the reinforced probes were described elsewhere [12]. The sole difference in the present case is that the steel rebars were not placed at the rotation axis of the mortar cylinder because four rebars were embedded per cylinder, as depicted in Fig. 1. The temperature of the seawater and the corrosion potential of the reinforcing bars was recorded every 20 s for more than 2 years (the experiment is still on-going). Periodically selected probes with surrounding seawater were temporarily transferred to the laboratory to perform controlled temperature cycles.

For the tests conducted in solutions (0.1 M NaOH) simulating the pH of concrete interstitial electrolyte, only the cross section of the AISI 304 SS rod was employed. The surface was polished with SiC paper abrasion down to grade 1200, followed by rinsing in ethanol and distilled water.

Electrochemical data (corrosion potential) were collected in the laboratory, in a three-electrode electrochemical cell, using a potentiostat (Ecochemie PGStat 30), and in the field, using a remote data logger. The reference electrodes were the saturated calomel, SCE, in all cases. An external salt bridge was employed when necessary to keep the reference electrode at constant temperature.

X-ray Photoelectron Spectroscopy (XPS) measurements were performed using a Microlab 310 F (Thermo Electron – former VG Scientific) equipped with a Mg (non-monochromated) anode and a concentric hemispherical analyser.

The XPS analysis was performed under pressures below 5×10^{-9} mbar, using an Al radiation (no-monochromator). The spectra were taken in CAE mode = 30 eV and accelerating voltage of 15 kV. The quantification was determined after peak fitting. The peak fitting function used was a Gaussian–Lorentzian product function and the algorithm was based on the Simplex optimization as used in the Avantage® software.

The XPS analyses were performed immediately after immersion of the probes in the testing solution in order to avoid any unwanted transformations of the passive layers formed.

3. Results and discussion

The open circuit potential of the reinforced concrete/mortar specimens was monitored in a nearly continuous mode (every 20 s). As shown in Fig. 2A, the corrosion potential underwent long-term variations, but also daily oscillations that were synchronised with the ambient sea water temperature changes. The 5 h delay marked in the figure can be attributed to the thermal inertia of the 2 cm mortar cover. The thermal dependence of the potential is approximately 1 mV °C^{-1} in this temperature range, which cannot be attributed to thermodynamic factors (Nernst law) or oxygen gradients in the confined pore network of concrete. The temperature

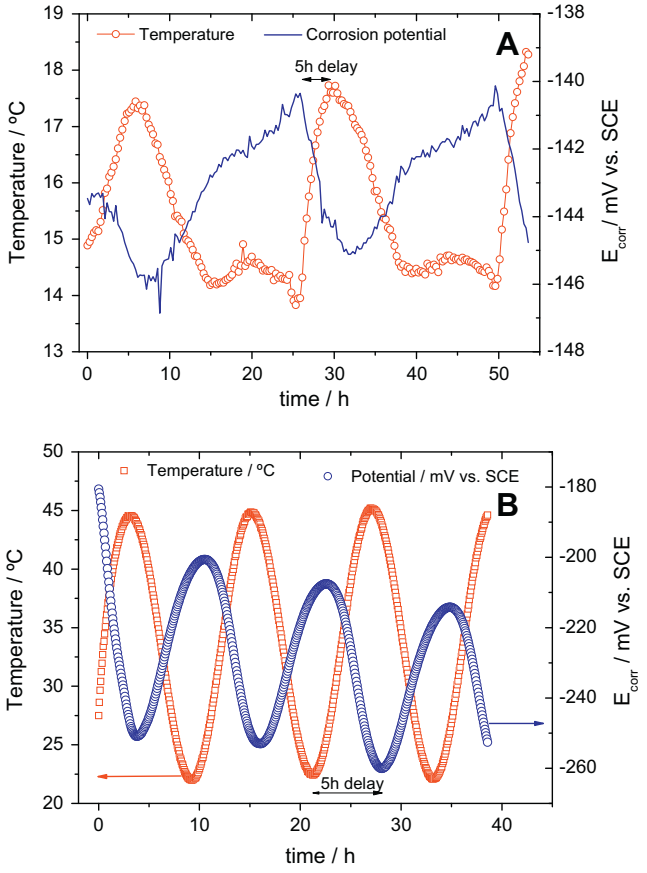

Fig. 2. Typical time records of temperature and corrosion potential of an AISI 304 stainless steel embedded in mortar after 2 years exposure in seawater. (A) Natural exposure site. (B) Laboratory condition (concrete probe temporarily transferred to the laboratory).

coefficient for the oxygen reduction reaction is given by Eq. (1), if the oxygen concentration and pH are considered constant in the narrow temperature range (~5 °C) measured in the field exposure site.

$$\frac{dE_{O_2}}{dT} = \frac{R}{4F} \ln \frac{C_{O_2}}{[OH^-]^4} \quad (1)$$

From Eq. (1), the thermal coefficient dE/dT ranges between 0.2 and 0.02 mV °C^{-1} for concrete pore solution pH between 12 and 13, respectively. The oxygen concentration in the pore solution is considered in equilibrium with that of the seawater, 0.23 mmol L^{-1}.

The same periodic temperature dependence was observed in laboratory conditions, by keeping the temperature within the intended controlled ranges. Fig. 2B depicts the results obtained on a reinforced concrete probe immersed in a seawater pool, in which the temperature was varied between 22 and 45 °C for a 24 h period. The temperature dependence of the potential was similar to that found for the lower temperature range (natural exposure conditions, Fig. 2A) but the thermal coefficient was approximately twice as high, ~2 mV °C^{-1}.

As the thermodynamic dependencies alone are not able to explain the observed potential variations, the next step in this research was to study the composition of the passive layer and how temperature affects it. For this purpose, tests in simulating concrete pore solutions (NaOH solution with pH identical to that of concrete) were conducted. The reason to choose that solution is to have a passive film representative of the real exposure conditions, but free of salt deposits, which normally hinder relevant

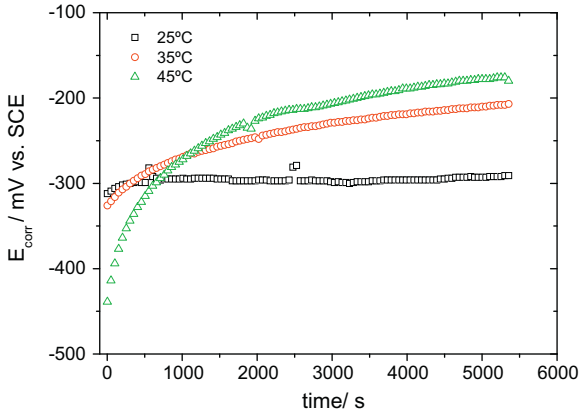

Fig. 3. Evolution of the open circuit potential with immersion time for AISI 304 stainless steel samples immersed in 0.1 M NaOH solution at 25, 35 and 45 °C.

information concerning the detailed passive films composition. This approach had been commonly used to carry analytical and electrochemical studies and very interesting insights were found by different authors [13,14].

There is abundant literature showing that pH (and potential) are relevant parameters defining the passive behaviour of iron and iron-base alloys [15,16]. Moreover, there are references demonstrating that no chloride incorporation occurs in the passive film even after several weeks of exposure [17].

Fig. 3 depicts the variation of the corrosion potential vs. time obtained for the three temperatures tested. At 25 °C, the corrosion potential of the AISI 304 SS remained stable during the testing period. However, for 35 and 45 °C the potential shifted in the noble direction as the immersion time increased. In fact, after stabilisation (approximately 1.3 h), Fig. 3 shows that the corrosion potential increased with the temperature; the same trend was observed for the buried steel samples.

At the beginning of the immersion period, the more negative potential was recorded for 45 °C temperature, which can be attributed to the lower oxygen concentration in solution. In fact, Fig. 3 shows that the corrosion potential cannot be defined solely by the chemistry of the solution. Therefore, additional processes at the metal concrete interface also seem to contribute significantly to explain the observed variations.

Literature had shown that in alkaline media (as in concrete's pore solution), passive films of iron and iron-based alloys demonstrate redox behaviour based on magnetite [18–20]. Magnetite oxidation leads to increased surface resistivity and thus shifts the corrosion potential in the nobler direction. The process is usually called "ageing" of the passive film. Usually the trend is characterised by potential/time profiles similar to those presented in Fig. 3, although the time scale very much depends on the surface conditioning procedures [17,21].

Figs. 4 and 5 depict the XPS ionisations for Fe2p3 and O1s, respectively, after immersion at 25 and 45 °C, according to Fig. 3. The XPS spectra were taken without previous sputtering, thus showing the chemical composition averaged over the size of the radiation spot (2 × 2 mm) and the penetration depth of the incident radiation (2–4 nm). Fig. 4 depicts the Fe2p3 ionisation spectra. The experimental spectra can be deconvoluted into the contributions of Fe^0, Fe^{2+}, and Fe^{3+} (with Fe^{3+} appearing in two forms, oxide and hydroxide). The contribution from Fe^0 indicates that the thickness of the passive film was uneven, with thinner areas through which the electrons from the substrate could be detected. This reveals that in this averaged area, the passive film can be very thin (a few nm only). The presence of Fe^{2+} can be assigned to magnetite or Fe^{2+} oxides. Fig. 4I (25 °C) and 4II (45 °C) reveal that the intensity of the peak corresponding to Fe^{2+} (710.18 eV) decreased as the temperature increased, while the opposite occurred for the peak associated with Fe^{3+}-oxide (711.58 eV). This suggests further oxidation of the passive film with temperature. Moreover, Fig. 5 shows the O1s ionisation that reveals a small shift towards higher energies and therefore the formation of more hydrated species.

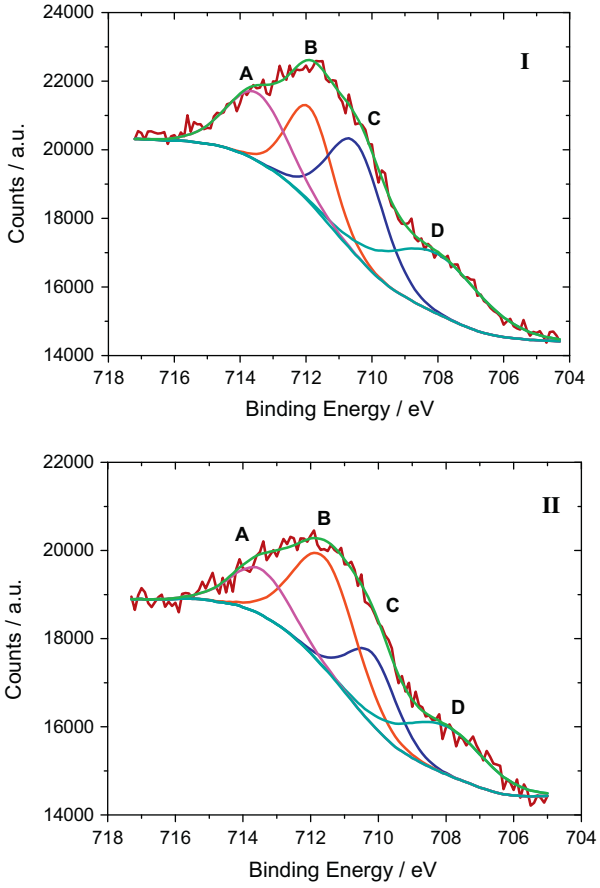

Fig. 4. XPS spectra corresponding to the Fe species found at the electrode's surface after 1.5 h immersion. The deconvolution peaks correspond to (A) Fe^{3+}-hydroxide (713.47 eV). (B) Fe^{3+}-oxide (711.58 eV), (C) Fe^{2+} (710.18 eV), and (D) Fe° (708.04 eV), and (I) at 25 °C (II) at 45 °C.

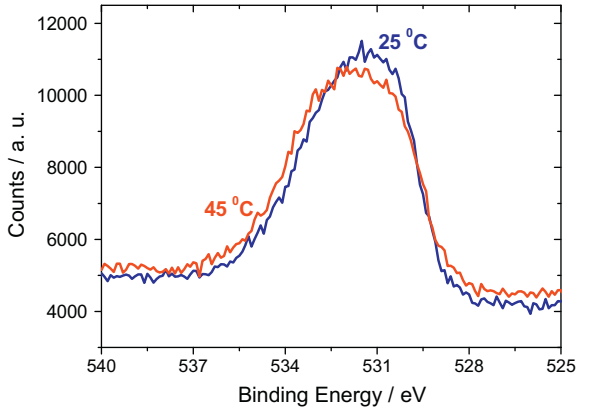

Fig. 5. XPS spectra corresponding to the O1s ionization for the films formed at 25 and 45 °C after 1.5 h immersion.

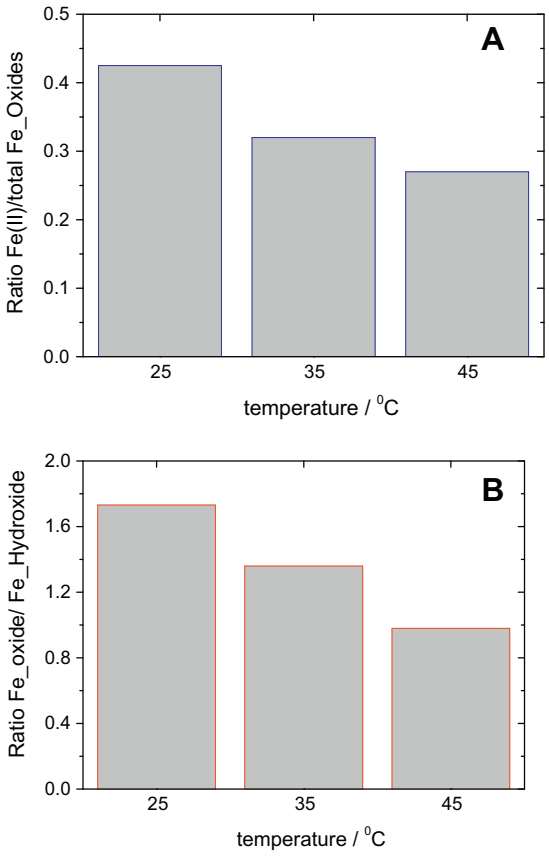

Fig. 6. Data obtained from the XPS spectra in the Fe energy window, corresponding to the Fe species found at the electrode's surface after 1.5 h immersion. (A) Ratio (Fe^{2+}/total oxides) vs. temperature and (B) ratio ($Fe_{oxide}/Fe_{hydroxide}$) vs. temperature.

Fig. 6A and B summarise the quantitative analysis of the XPS spectra. The evident conclusion from these figures is that the passive film formed on the AISI 304 SS was sensitive to the temperature. The film underwent oxidation (Fig. 6A) and hydration (Fig. 6B) as the temperature increased.

Assuming that magnetite is the main iron compound forming the passive film in the tested conditions, the following redox processes [22] can be considered to be involved in the temperature-induced transformations:

(a) Oxidation and dehydration of the Fe(II)-rich film

$$\text{Formation of maghemite}: 2Fe_3O_4 + 2OH^- \rightleftharpoons 3\gamma - Fe_2O_3 + H_2O + 2e^- \quad (2)$$

$$\text{Formation of hematite}: 2Fe_3O_4 + 2OH^- \rightleftharpoons 3\alpha - Fe_2O_3 + H_2O + 2e^- \quad (3)$$

(a) Oxidation and hydration of the Fe(II)-rich film

$$\text{Formation of lepidocrocite}: 2Fe_3O_4 + OH^- + H_2O \rightleftharpoons 3\gamma - FeOOH + e^- \quad (4)$$

$$\text{Formation of goethite}: 2Fe_3O_4 + OH^- + H_2O \rightleftarrows 3\alpha - FeOOH + e^- \quad (5)$$

According to the experimental data reported in Fig. 6B, the magnetite oxidation occurs through the processes described in Eqs. (4 and/or 5). This result is relevant because hydrated passive films are more resistant to chloride attack due to local decreasing of the Cl^-/OH^- ratio [23], and because the oxidation products themselves can act as depolarisers of the cathodic reaction [24], which explains the observed temperature dependence of the corrosion potential. The coupled cathodic and anodic reactions (during the rising and decreasing temperature cycles, respectively) will probably be oxygen reduction (Eq. (6)) and substrate oxidation (Eq. (7)).

$$O_2 + 2H_2O + 4e^- \rightarrow 4OH^- \quad (6)$$

$$Fe \rightarrow Fe^{2+} + 2e^- \quad (7)$$

In this way, temperature oscillations boost the corrosion reaction during the decreasing semi-cycle (Eqs. (7) and reverse 4, 5) and modify the structure of the film during the rising semi-cycle (Eqs. (4)–(6)). The increase in the temperature coefficient ($mV\ °C^{-1}$), as the average temperature increased, can be understood in terms of larger transformation of the magnetite-based passive layer, whose electrode potential is proportional to the Fe^{3+}/Fe^{2+} ratio in the oxide film [25].

The temperature-induced structural changes in the passive layer are expected to have major effects on the long term corrosion performance of the steel because of decreased barrier properties and film thickening. The decreased barrier properties will be a direct consequence of the quite large differences in density of the iron oxides involved in the redox processes discussed above.

4. Conclusions

Temperature-induced corrosion potential oscillations were investigated for AISI 304 SS in alkaline solution and in mortar. Natural and laboratory tests showed that the corrosion potential followed the ambient temperature variations. Analytical (XPS) data demonstrated that those potential variations were associated with changes in the composition of the passive film, which were interpreted in terms of redox processes of the iron oxides present in the passive layer.

From the point of view of the life expectancy of reinforced concrete structures, it seems clear that environment temperature oscillations should have an important effect in the stability and protection efficiency of the passive film and thus it should be incorporated in corrosion behaviour models.

Acknowledgement

This work was partially supported by the Spanish *Ministerio de Economía y Competitividad* through the project BIA2010-16950. The financial support from the project PTDC/ECM/69132/2006 is also acknowledged.

References

[1] D.D. Macdonald, J. Electrochem. Soc. 153 (2006) B213.
[2] J. Brigham, E.W. Tozer, Corrosion 29 (1973) 33.
[3] R.J. Brigham, E.W. Tozer, Corrosion 30 (1974) 161.
[4] M.H. Moayed, N.J. Laycock, R.C. Newman, Corros. Sci. 45 (2003) 1203.
[5] 5 ASTM G150 – 99(2010) Standard Test Method for Electrochemical Critical Pitting Temperature Testing of Stainless Steels. Available at <http://www.astm.org/Standards/G150.htm>.
[6] G.T. Burstein, J.J. Moloney, Electrochem. Commun. 6 (2004) 1037.
[7] A.C. Lloyd, D.W. Shoesmith, N.S. McIntyre, J.J. Noel, J. Electrochem. Soc. 150 (2003) B120.
[8] Y. Ashida, L. Glen McMillion, M.L. Taylor, Electrochem. Commun. 9 (2007) 1102.
[9] W. López, J.A. González, C. Andrade, Cem. Concr. Res. 23 (1993) 1130.
[10] V. L'Hostis, E. Amblard, C. Blanc, F. Miserque, C. Paris, L. Bellot-Gurlet, Corros. Eng. Sci. Technol. 46 (2011) 177.
[11] C. Andrade, C. Alonso, J. Sarria, Cem. Concr. Compos. 24 (2002) 55.
[12] C. Andrade, L. Soler, C. Alonso, X.R. Nóvoa, M. Keddam, Corros. Sci. 37 (1995) 2013.
[13] L. Freire, M.J. Carmezim, M.G.S. Ferreira, M.F. Montemor, Electrochim. Acta 56 (2011) 5280.

[14] A. Bautista, G. Blanco, F. Velasco, A. Gutiérrez, L. Soriano, F.J. Palomares, H. Takenouti, Corros. Sci. 51 (2009) 785.
[15] C. Alonso, M. Castellote, C. Andrade, Electrochim. Acta 47 (2002) 3469.
[16] W.H. Hartt, J. Nam, Corrosion 64 (2008) 671.
[17] C.M. Abreu, M.J. Cristóbal, R. Losada, X.R. Nóvoa, G. Pena, M.C. Pérez, Electrochim. Acta 51 (2006) 1881.
[18] B. MacDougall, M.J. Graham, Growth and stability of passive films, in: P. Marcus, J. Oudar (Eds.), Corrosion Mechanisms in Theory and Practice, Marcel Dekker Inc., NY, USA, 1995, pp. 143–173.
[19] C. Andrade, M. Keddam, X.R. Nóvoa, M.C. Pérez, C.M. Rangel, H. Takenouti, Electrochim. Acta 46 (2001) 3905.
[20] M. Sánchez, J. Gregori, C. Alonso, J.J. García-Jareño, H. Takenouti, F. Vicente, Electrochim. Acta 52 (2007) 7634.
[21] D. Addari, B. Elsener, A. Rossi, Electrochim. Acta 53 (2008) 8078.
[22] S. Joiret, M. Keddam, X.R. Nóvoa, M.C. Pérez, C. Rangel, H. Takenouti, Cem. Concr. Compos. 24 (2002) 7.
[23] A. Collazo, M.J. Cristóbal, X.R. Nóvoa, G. Pena, M.C. Pérez, J. ASTM Int. 3 (2006) JAI11785.
[24] C. Alonso, C. Andrade, M. Izquierdo, X.R. Nóvoa, M.C. Pérez, Corros. Sci. 40 (1998) 1379.
[25] M. Sánchez-Moreno, H. Takenouti, J.J. García-Jareño, F. Vicente, C. Alonso, Electrochim. Acta 54 (2009) 7222.